Heritage Science

RESEARCH

Open Access

Deterioration-associated microbiome of a modern photographic artwork: the case of *Skull and Crossbones* by Robert Mapplethorpe

Mariagioia Petraretti[1,9*], Antonino De Natale[1], Angelo Del Mondo[1], Romualdo Troisi[7], Olga De Castro[2,3,4], Nicolina Mormile[1], Mariano Avino[5], Gennaro Tortino[6], Giuseppe Oreste Graziano[6], Alessandro Vergara[7,8] and Antonino Pollio[1*]

Abstract

The preservation of cultural heritage, including ancient photographic materials, is of paramount importance in the field of conservation science**.** In this context, the microbial diversity of 'Skull and Crossbones', a 1983 photograph by Robert Mapplethorpe printed on silver gelatine, was assessed. We employed both culture-dependent and culture-independent methods to characterize microbial communities inhabiting this artwork. Vibrational Raman micro spectroscopy and FT-IR spectroscopy were utilized to assess the chemical degradation condition and characterize the chemical components of the silver gelatin print. The combination of molecular sequencing methods (Sanger and HTS approach) and non-invasive vibrational spectroscopy yielded valuable insights into the microbial communities thriving on photographic material and the chemical degradation of the print. Isolated fungal strains were added to the Fungal Collection at the University of Naples Federico II, and their deteriorative potential was investigated by adding substrates, commonly used in canvas photographs to the culture media. These results establish a link between microbial communities colonizing ancient photographic materials, paper decomposition, and the enzymatic patterns of the retrieved microorganisms. This information is invaluable for understanding and addressing biodeterioration progression on valuable works of art, such as historical photographs, which remain understudied.

Keywords Fungi, Biodeterioration, High, Throughput sequencing, Raman microspectroscopy, Historical photographs, Prokaryotes

*Correspondence:
Mariagioia Petraretti
mariagioia.petraretti@unina.it
Antonino Pollio
antonino.pollio@unina.it
[1] Department of Biology, University of Naples Federico II, Via Cintia 26, 80126 Naples, Italy
[2] Department of Biology, University of Naples Federico II, Via Foria 223, 80139 Naples, Italy
[3] Botanical Garden, Via Foria 223, 80139 Naples, Italy
[4] DNATech Srl, Botanical Garden, Spin-off Company of the University of Naples Federico II, Via Foria 223, 80139 Naples, Italy
[5] Department of Biochemistry and Functional Genomics, Sherbrooke University, 3201 Jean Mignault, Sherbrooke, QC J1E 4K8, Canada
[6] Royal Palace of Caserta, Caserta, Italy
[7] Department of Chemical Sciences, University of Naples Federico II, Via Cintia 26, 80126 Naples, Italy
[8] Task Force di Ateneo "Metodologie Analitiche per la Salvaguardia dei Beni Culturali", Naples, Italy
[9] Present Address: Department of Food, Environmental and Nutrition Sciences, Università degli Studi di Milano, Milan, Italy

Introduction

Biodeterioration of modern artworks

Historical photographs represent valuable works of art with a finite life due to the process of biodeterioration. Photographic prints are susceptible to spontaneous deterioration, primarily due to the instability of silver images. Concerns related to their preservation date back to the early times of photography [1]. In fact, internal factors may initiate the decay process, which is subsequently exacerbated by external factors, such as inappropriate selection of enclosure materials and unfavorable environmental conditions, including high relative humidity, and UV light exposure [2].

The rise of photographic materials as a cultural asset has been primarily observed over the last two centuries. Several techniques have been used to produce photographic materials, but in general they mainly consist of two components: a support structure and a photosensitive emulsion [3]. The support often includes image-forming material, such as silver particles for black and white images and a binder [4], which is usually gelatin or albumin. Gelatin and albumen are two common binders in historical photographs, each offering distinct properties. Gelatin became popular at the end of the 19th century, and thanks to its versatility and stability, gelatin silver prints dominated black and white photography in the 20th century Albumen, predating gelatin, was extensively used in the mid-19th century for albumen prints, known for their rich tonal range and sharp detail. These binders played a crucial role in the construction of photographic prints, aiding in the adhesion of light-sensitive emulsions to various substrates such as paper, glass, or metal [5].

In the context of photographic films, various carriers have been used, such as cellulose nitrate, cellulose diacetate, cellulose triacetate, and polyethylene terephthalate. These components make photographic materials susceptible to microbial attack, particularly by fungi with cellulolytic and proteolytic activities. Fungi can indeed degrade photographs and films through hyphal penetration, attacking and breaking down the binder, leading to irreversible decay [6]. Fungal colonies may also manifest as colored spots, leading to a loss of image sharpness, while oxidants and pigment deposition are the main culprits for staining and yellowing of photograph material [7].

However, high environmental relative humidity can lead to gelatin softening and subsequent increased solubility, resulting in changes in print brightness and detachment from the paper [8]. Both gelatin and paper serve as the primary energy source sustaining biofilm metabolisms; biofilms actively dissolve gelatin and induce chemical alterations in the silver particles within the emulsion, thus causing gradual photograph dissolution. Both bacterial and fungal communities are responsible for attacking photographs, with the former being particularly destructive [9, 10]. Recent research has highlighted the compartmentalization of different species within biofilms, each occupying separate niches [11].

Until recently, the conservation and restoration of photographs received limited attention and were often treated as a distinct case of paper biodeterioration. The subject of this study is a silver gelatin printed photograph namely *Skull and Crossbones*, by Robert Mapplethorpe which is on permanent exhibition and visited by thousands of people annually at the Royal Palace of Caserta (CE, Italy). While it is generally recommended to store photographs in cool and dry environments with minimal light exposure to prevent biodeterioration, this is not feasible for Mapplethorpe's artwork, as the environmental conditions present a significant challenge to museum staff.

The photograph under study showed damages attributable to active biological degradation, and subsequently this study, it has undergone a restoration intervention. The objective of the study was to assess the extent of photo decay through a detailed diagnostic analysis. The correlation between microbial colonization and photographic material damage remains poorly understood [12], yet this information is essential for designing effective restoration approaches.

To achieve this, we first evaluated the extent of resident microbial community on the artwork, identifying the species composition of the biofilm using both culture-dependent and -independent methods. While culture techniques are valuable for characterizing biofilm microorganisms, they are insufficient for assessing microbial diversity and the overall abundance as many of microorganisms in biofilms are uncultivable [13]. Therefore, we complemented them with culture-independent techniques [14].

Culture-dependent methods were employed to isolate and identify microorganisms sampled from the artwork's substrates, followed by Sanger sequencing to determine their degradation potential. However, since not all microorganisms in biofilm samples are known to contribute to active biodeterioration, we conducted analyses to understand the degradation patterns of isolated microorganisms, focusing on their cellulolytic and proteolytic activity [15].

As a culture-independent method, High-Throughput Sequencing (HTS) was employed to obtain a comprehensive representation of bacteria and fungi inhabiting the Mapplethorpe's artwork as a whole biofilm at higher taxonomic levels.

Further over, we performed vibrational spectroscopic measurements on photographic samples (Raman spectroscopy for the front, and FTIR spectroscopy for the back) to assess the extent of chemical damage resulting from the presence of bacterial and fungal communities. This non-invasive microanalysis technique has been successfully employed to study alterations in photographic materials [16].

The present work represents the first characterization study of the microbial community and chemical degradation state of an artwork from the Terrae Motus modern art collection, thereby serving as a guide for subsequent research endeavors. To date, only a few studies have considered the features and mechanisms of biological degradation of photographic artworks, as further discussed below in this work. Additionally, it is worth noting that until now, the few published works on photographic artworks have focused either solely on microbial characterization or solely on their chemical degradation, without simultaneously considering both aspects [17–22]. The combined approach used in this study paves the way for a far-sighted non-invasive methodology to study modern non-conventional artworks, such as photographs. Beside the identification of associated microbiomes and their degradative potential – intended as the capacity to break the cellulose and gelatin support, as well as the deposit of pigments – the spectroscopic methods here applied show the potential to map the severity of degradation degree, thus opening the route to the set-up of novel non-invasive diagnostic methods for the preservation of photographic material cultural heritage.

Material and methods

The *terrae motus* collection and robert mapplethorpe's photographs

The *Terrae Motus* Collection was established by Neapolitan art gallerist Lucio Amelio (1931–1994) in the early 1980s, following the massive earthquake in Campania and Basilicata dated November 23rd 1980. Amelio conceived the *Terrae Motus* project, centered on the theme of natural catastrophes, and invited 66 international artists, who collaborated with his gallery, the Modern Art Agency**,** to create artworks on this subject. Featuring renowned artists like Barceló, Cragg, Warhol, and Mapplethorpe, the collection debuted in 1984 at Villa Campolieto in Ercolano (Naples), and later traveled to Paris in 1987 before finding a permanent home at the Royal Palace of Caserta. One notable installation by Robert Mapplethorpe from the collection includes five black and white photographic prints, with the central photograph, "*Skull and Crossbones*" exhibiting significant signs of biodeterioration after nearly 40 years on display, prompting a comprehensive conservation assessment. Mapplethorpe's five sequence of photographs emulates the images of a polyptych and alludes to traditional religious paintings. The references to the symbols of Christ's passion are clear, such as: the crown of thorns in Jack with crown; and the profile of Magdalene in Jill Chapman. The shots were all taken in the artist's studio except for the central image with the skull, *Skull and Crossbones*, which was taken by Mapplethorpe in front of the church of *Santa Maria delle Anime del Purgatorio ad Arco* in via dei Tribunali, during one of his stays in Naples. The photos were printed, in all probability, by Tom Baril (1952), a historic printer, with whom Mapplethorpe collaborated since 1979 for the very high quality of his work, who continues to print the artist's works for the Mapplethorpe Foundation. The work was exhibited for the first time in Boston, at the Institute of Contemporary Art, in November 1983; later, together with all the other works of *Terrae Motus* at Villa Campolieto (Ercolano, Naples) in 1984. The state of conservation of the works was compromised by the diffused colonization by potentially biodeteriogenic microbial agents. The image layer of the photographs has been damaged by the metabolic action of the microbial community, in some cases irreversibly, compromising the aesthetics and correct perception of the work. In particular, the *Skull and Crossbones* print, for conservation reasons, can no longer be re-exhibited, paving the way for new solutions to reconstitute the aesthetic unity of the installation.

Sampling

Sampling was performed on the photo named *Skull and Crossbones* (Fig. 1).

To the naked eye, the photograph was extensively affected by microbial contamination on back of the photograph (BC) and, to a lesser extent, also on front of the photograph (FC). Two and four samples were respectively taken from the front and back canvas in two ways: (1) by gently pressing 2×2 cm adhesive tape samples on photographic material, which were immediately attached to autoclaved slides. From this second set of samples, approximately 1 cm of the tape was then cut using sterile blade, removed with sterile tweezers, and inserted into 2 mL tube tubes, which were used for HTS; (2) with sterilized cotton swabs that were deposited into sterile vials, transported at 4 °C and then stored at − 20 °C. These samples were used for DNA barcoding characterization using Sanger sequencing.

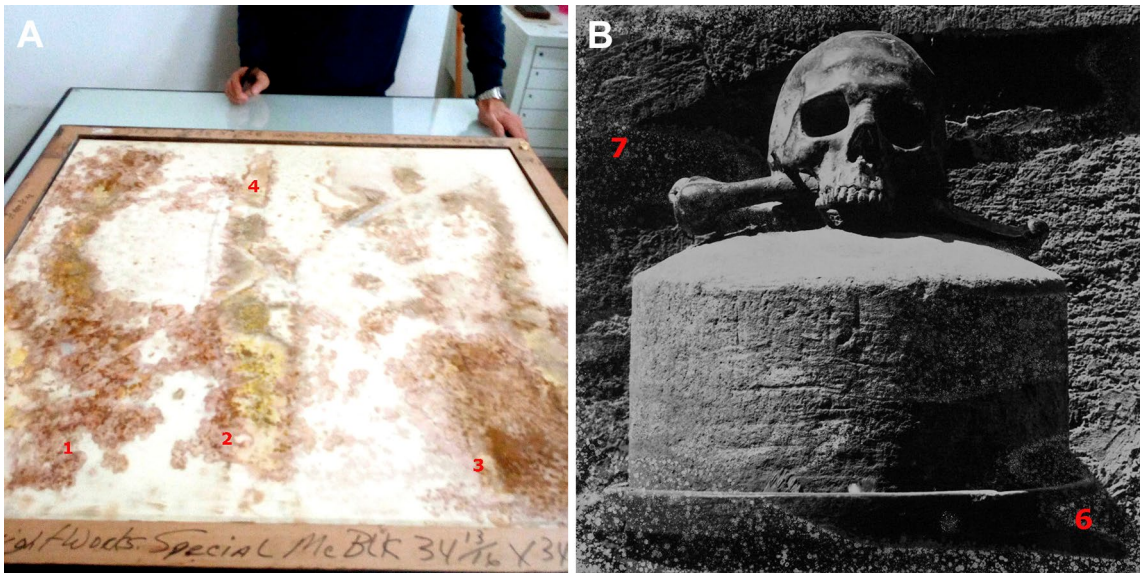

Fig. 1 Sampling on *Skull and Crossbones* photograph on back of the photograph (BC) samples n.o. 1–4 (**A**) and on front of photograph (FC) samples n.o. 6–7 (**B**)

DNA barcoding analyses

SANGER sequencing

Isolation of bacterial and fungal strains Each sterile swab used for sampling was added to 1 ml of sterile distilled water, then decimal dilutions were performed in triplicate. After dilutions, 100 µL were plated on dishes containing 30 mL of agarized Potato Dextrose medium (PDA, Merck, Germany) with chloramphenicol (0.1%) and 30 mL of agarized Tryptic Soy medium (TSA, Merck, Germany) with nystatin (0.2%) to isolate total fungi and bacteria, respectively. The PDA plates were incubated at 25 ± 2 °C for ten days, while the TSA plates were incubated at 28 ± 2 °C for 72 h. Once dishes were incubated, fungal and bacterial colonies were counted. Colony forming units expressed in CFU/cm^2 were determined. The result was calculated as the arithmetic mean of 3 independent repetitions. Then, individual colonies were pinched and repeatedly streaked onto agar plates to obtain pure cultures. The isolation of fungi was carried out with a sterile needle under a dissecting microscope. Fungal strains were cultivated using a culture medium PDA, while bacteria strains were cultivated on TSA. All the isolates were added to the novel fungal collection at University of Naples Federico II, namely FCUF [23].

Genomic DNA extraction, amplification, and identification of isolates DNA was extracted from each isolate with a modified DNA extraction protocol [24] and used for a Polymerase Chain Reaction with primers targeting the bacterial 16S rRNA gene (16S_forward: 5′-AGGATG CAAGCGTTATCCGG-3′; 16S_reverse: 5′-AATCCC ATTCGCTCCCCTAG-3′) and the fungal Internal Transcribed Spacer region, including 5.8S gene (ITS1 5′-TCC GTAGGTGAACCTGCGG-3′; ITS4: 5′- TCCTCCGCT TATTGATATGC-3′). Additional regions, b-tubulin (Bt2a5′-GGTAACCAAATCGGTGCTTTC-3′;Bt2b 5′-ACCCTCAGTGTAGTGACCCTT-3′) and translation elongation factor 1-a (EF1-728 forward 5′-CATCGAGAA GTTCGAGAAGG and TEF1_reverse TACTTGAAG GAACCCTTACC) were amplified to ensure a robust molecular identification of fungal isolates. Amplification reaction was carried out in a reaction volume of 25 µL containing a buffer reaction (1/10 volume of the supplied 10×buffer), a deoxynucleoside triphosphate mixture (0.2 mM each), supplemented of 2.5 mM MgCl2, 0.5 mM of each primer and 1.25 U of Taq polymerase (EconoTaq, Lucigen). One microliter of DNA (ca. 10 ng) was added to each reaction mixture, then the PCR reactions were run in a thermocycler (Applied Biosystems 2720, Thermo Fisher Scientific) according to conditions described for 16S gene [25], ITS 1–4 [26], BTUB [27], and TEF1 [28]. Amplicons were purified using PEG8000 precipitation (PEG 15%, NaCl 2.5 M) and were sequenced using Bright Dye Terminator Cycle Sequencing Kit (ICloning). The amount of primer and template in a cycle sequencing reaction was according to the manufacturer's instruction. The reactions were purified using BigDye Xterminator Purification Kit (Applied Biosystems, Thermo Fisher Scientific) and 13 µL of template was run in an automated sequencer (3130 Genetic Analyzer, Life Technologies, Thermo Fisher Scientific). The characterization of the isolated strains was made employing BLASTN (Basic Local Alignment

Search Tool-Nucleotide, https://blast.ncbi.nlm.nih.gov/Blast.cgi), identifying the microorganisms by choosing the highest percentage of identity with a 99% cut-off for both bacteria and fungi. A minimum E-value lower than $E^{-4}$was considered. All ITS and 16S sequences were submitted to GenBank.

High-throughput sequencing

Microbial genomic DNA extraction and PCR amplification

Four adhesive tapes from back of the photograph and two from front ca of the photograph were used for the DNA extraction (see point 1 in Sampling paragraph). Total DNA of the sampled microbial community was extracted from around 1 cm of adhesive tape using a modified protocol according to [29] (Additional file 1., Appendix S1). The DNA was resuspended in 20 µL of which 1 µL was analysed using a Qubit 3 Fluorometer (Invitrogen, Thermo Fisher Scientific) to determine the DNA concentration. To compare the Prokaryotes (archaea and bacteria) and fungi community composition and diversity in each adhesive tape sample, amplicon surveys of a portion of the partial 16S rRNA gene (targeting V3-V4 regions) and the intergenic transcribed spacer (targeting ITS2) were performed (respectively). The barcoded primer sets for 16S rRNA gene were Pro341F (5′-CCT ACG GGN BGC ASC AG-3′) and Pro805R primers (5′-GAC TAC NVG GGT ATC TAA TCC-3′) [30] and for ITS2 nuclear marker were ITS3 (5′-GCA TCG ATG AAG AAC GCA GC-3′) and ITS4 primers (5′-TCC TCC GCT TAT TGA TAT GC-3′) [31], respectively. Both forward and reverse primer contained Illumina overhang adapter sequences (5′-TCG TCG GCA GCG TCA GAT GTG TAT AAG AGA CAG-3′ + forward primer; and 5′-GTC TCG TGG GCT CGG AGA TGT GTA TAA GAG ACA G-3′ + reverse primer). After several optimization amplification tests, PCR was made in a 40 µL reaction mixture consisting of 2 µl of DNA template (ca. 0.5–3 ng) and Kodaq 2X PCR MasterMix (Applied Biological Materials Inc., ABM) with 0.25 mM of each primer. The reaction conditions were as follows: an initial denaturation step of 94 °C for 3 min and then 35 cycles of denaturation at 94 °C for 30 s, annealing at 55 °C for 30 s and extension at 72 °C for 30 s. The final extension was performed at 72 °C for 5 min. A negative control without DNA was employed for each primer combination. A duplicate for each amplicon was carried out for reproducibility purposes. To remove possible microbial DNA contaminating from MasterMix and water, a modified pre-treatment before the PCR reaction was carried out using 2.5 U of Bsp143I (Sau3AI) (Thermo Fisher Scientific) for 37 °C for 30 min (plus 65 °C 20 min deactivation) [26]; a positive control of digestion reaction was also carried out using as DNA template 300 ng of pGem-3Zf + (Applied Biosystem, Thermo Fisher Scientific). The amplicons were quality checked and quantified using the UVIdoc HD5 gel documentation system (UVITEC) and a Qubit 3 Fluorometer, respectively. A quantitative of 25 µL (> 5 ng/µL) of each amplicon was shipped to BMR Genomics s.r.l. (Padua, Italy) for sequencing using a MiSeq platform (2 × 300 paired-end sequencing; 2 × 50,000 reads/sample) (Illumina).

High-throughput sequencing data analyses

MiSeq pair ends data from ITS2 (fungi) and 16S (Prokaryotes) were obtained from six samples corresponding to two samples from the front of the canvas (FC) and four from the back of the canvas (BC), including a replicate for each sample. Sequences were quality checked with subsequent adapter removal using Trim Galore 0.6.1 (http://www.bioinformatics.babraham.ac.uk/projects/trim_galore/). PEAR v0.9.8 [32] was utilized to merge pair-end reads. ITS2 was extracted for fungi using ITSx v1.0.11 [33]. VSEARCH v1.11.1 [34] was utilized to eliminate chimeras by running our sequences through a dedicated chimeric database employing the UCHIME algorithm [35]. All subsequent analyses were performed with QIIME v1.9.1 [36].

OTUs were picked using the script pick_open_reference_otus.py from QIIME with '–suppress-align-and-tree' flag employing the reference and taxonomy databases version 'sh_refs_qiime_ver8_dynamic_all_02.02.2019' (https://unite.ut.ee/repository.php#uchime) for ITS2, '97_otu_taxonomy.txt' default from QIIME for 16S. Statistically tests to determine whether there is statistical significant difference between groups (in our case between the front and back canvas and between sample replicates) were performed inside QIIME using the non-parametric test ANOSIM with 999 permutations using a Bray-Curtis distance metric [37]. This test returns a p-value which represents the proportion of permutations that yielded an ANOSIM test statistic (called R) that is equal or stronger than the R calculated from the actual data.

Degradation potential of isolated microorganisms

Cellulolytic activity of fungal isolates

The ability of fungal isolates to produce cellulases was determined following the method described by Teather and Wood (1982) using carboxymethyl cellulose (CMC 1%) agarized medium containing carboxymethyl cellulose 10 g; $NaNO_3$ 1 g; K_2HPO_4 1 g; $MgSO_4$.7H2O 0.5 g, KCl 1 g; $FeSO_4$ 0.1 g, agar 20 g and distilled water l L was prepared. The medium was sterilized at 121 °C for 20 min and, subsequently, poured into plates square under a sterile flow. One agar disk (8 mm diam.) of 6 days old cultures of each fungal isolate was placed in the center of

CMC plates and then incubated at 25 °C for 7 days. After incubation, plates are flooded with 1% Congo red dye and washed with 1 M NaCl after 15 min to stabilize the reaction [38]. Because Congo red stain is held by only integral cellulose polymers, cellulase activity was indicated by the clear zones around fungal growth [39]. A digital camera was used to capture photographs after staining the plates. Software ImageJ version 1.52 k [40] was used to measure fungal growth (as the diameter of the colony) and the diameter of the halo for subsequent calculation of the enzymatic index (EI), a semi-quantitative estimate of enzyme activity according to the following relation [38]: EI = Diameter of hydrolysis zone/Diameter of colony.

Proteolytic activity

Proteolytic activity was determined using gelatin hydrolysis assays [41]. The fungal strains were inoculated into a culture medium with the same composition as that used for the cellulolytic activity test, replacing CMC with 0.5% gelatin as sole carbon source. The medium was sterilized at 121 °C for 20 min.

Fungi were inoculated into gelatin-containing plates, running three spots for each, and incubated in a thermostat at 25 °C for 7 days. When fully developed, the hydrolysis of the gelatin is was highlighted following the procedure described by Vermelho [42]: the plates were coated with a 0.1% solution of black starch in methanol-acetic acid–water in the ratio 30:10:60 for 1 h at 30 °C and decoloring with a solution of methanol-acetic acid water, in the ratio 30:10:60 for 15 min; after removing the dye, the plates were flood with the bleach consisting of methanol + acetic acid + water (30:10:60) for 15 min to stabilize the reaction. Any areas of hydrolysis appear in the form of halos clarification.

Statistical analyses

All results were analyzed according to a completely randomized design with three replicates per sample. Analysis of variance (ANOVA) was used for the statistical analysis of the data, and significant differences were compared by Dunnett's test, using Prism software, from three independent replicate values. The value of $p \leq 0.05$ was considered statistically significant.

Vibrational spectroscopic analyses

Raman microspectroscopy

Raman microspectroscopy was carried out on the front page of the photograph. Indeed, during the analysis of the state of conservation of the photo, preliminary to the restoration intervention, sampling of microsections of the emulsion layer on the back of the photograph was carried out. The Raman spectra were collected at room temperature using a confocal micro-Raman spectrometer (Jasco, NRS-3100), working with the 514 nm excitation line from an Ar^+ laser (3 mW at the sample) in a backscattering configuration. The scattered light was analyzed with a spectrometer equipped with a Peltier-cooled 1024 × 128 pixel CCD photon detector (Andor DU401BVI). A holographic notch filter was used to reject the excitation laser line. Raman backscattering was collected using a diffraction lattice of 1200 grooves/mm and 0.01–0.20 mm slits, corresponding to an average spectral resolution up to 1 cm^{-1} [43]. Wavelength calibration was performed by using cyclohexane Raman signal as a reference. The spectra acquisition times varied from 30 to 90 s, and they were triplicated for scope of reproducibility. Assignment of Raman spectra was carried out by comparison with literature data and web database (e.g. RRUFF library).

FT-IR spectroscopy

Fourier-transform infrared spectroscopy was carried out on the back of the photograph. This sampling was carried out on some fragments of the secondary photographic support, subject to microbial infection. The secondary support was then replaced during the restoration work. FT-IR measurements were performed using a Nicolet system (model 5700 FT-IR spectrometer) in ATR mode. About 1–2 mg of sample was put on the optic window (ZnSe crystal). Spectra were collected in the range of 4000–600 cm^{-1}, 128 scans, and a resolution of 4 cm^{-1}.

Results

Molecular DNA analyses

SANGER sequencing

Culture-dependent isolations The number of culturable fungi on the photographs ranged from 2.6×10^5 CFU/cm^2 (Sample No. 1 back canvas) to 1.0×10^6 CFU/cm^2 (Sample No. 4 back canvas). A similar level of contamination was found on the front of the photograph, ranging from 1.1×10^5 CFU/cm^2 (Sample No.5 front canvas) to 2.1×10^5 CFU/cm^2 (Sample No.8 front canvas). Bacteria were the least numerous on the photographs, with their numbers ranging from 2.1×10^1 CFU/cm^2 (Sample No. 2 back canvas) to 1.6×10^2 CFU/cm^2 (Sample No. 6 front canvas). No algae nor cyanobacteria were retrieved from our samples.

DNA barcoding identification In total, nineteen fungal isolates and one bacterial isolate were recovered. Concerning the back side of the photograph, four distinct fungal species from three different genera were isolated. No bacterial strains were detected using the culture-dependent method from samples derived from the back of the photograph (Fig. 2).

As for the front front of the photograph, four distinct fungal from four different genera, plus one species of bacteria, were isolated (Fig. 3).

The recovered fungi belonged to Ascomycota (89%) and Basidiomycota (11%) phyla. The most abundant isolates belonged to the *Cladosporium* genus, followed by *Penicillium*. *Purpureocilium*, *Sporobolomyces* and *Paraconiothirium* genera were isolated in equal proportions. The genus *Chaetomium* was the least abundantly isolated.

The molecular identifications obtained with eukaryotic nuclear rRNA/ITS and prokaryotic 16S rRNA were submitted on Gene Bank. The processed accession numbers are OR816146-OR816164 for eukaryotic barcode (submission ID: SUB13982410), while the processed accession number is PP468626 (submission ID: SUB14304634) for prokaryotic barcode and are listed in Table 1.

Deteriorative potential

Given that not all microorganisms thriving on artworks pose a risk for their integrity and appearance, we investigated the enzymatic potential of the obtained isolates. Focusing solely on fungal isolates, given that they are generally more associated with deterioration compared to bacteria, all the fungal isolates showed cellulolytic activity, with enzymatic indices ranging between 0.8 ± 0.1 and 1.7 ± 0.1. However, not all isolates displayed a proteolytic activity (Table 2).

High-throughput sequencing

The percentage of reads that included adapters varied between 6.9% and 84.3% before their subsequent removal. Reads that did not pass the quality Phred score cutoff of 20 ranged from 2.5% and 24.4%. For the 16S analysis, the total number of OTUs spanned between 38,000 to approximately 94,000. After applying this filter, the median number of OTUs was 60,081.500. In the case of ITS2 analysis, the total number of OTUs ranged from 84,000 to around 173,000 reads, a median of 129,946.000.

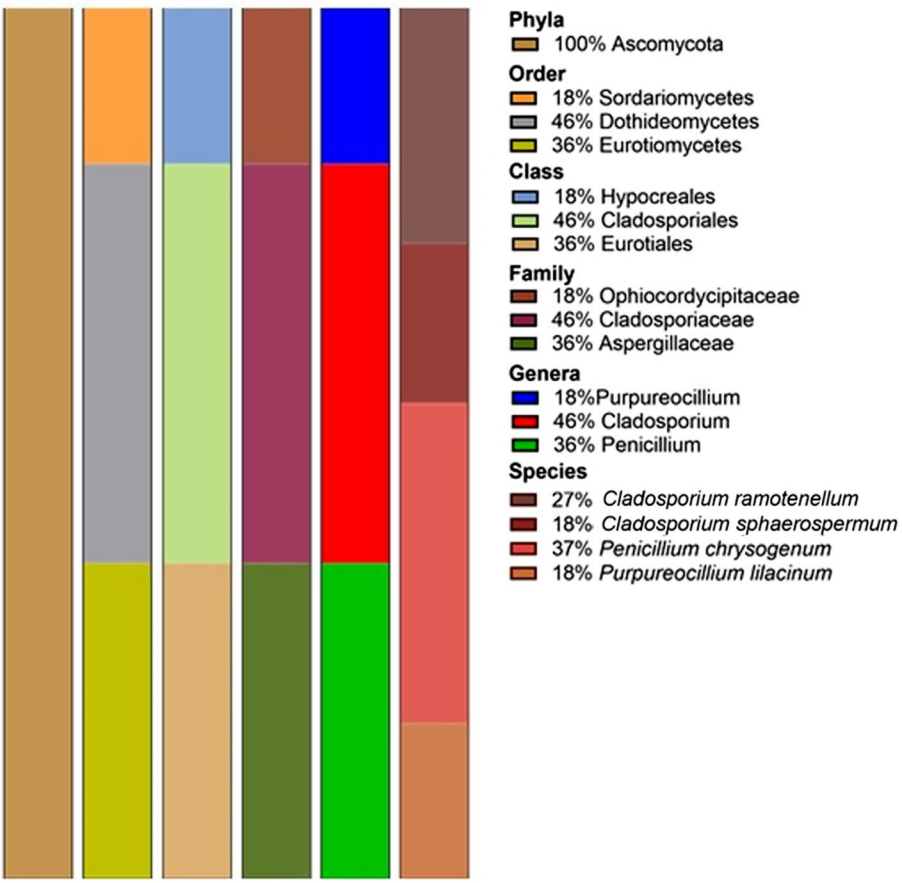

Fig. 2 Proportions of retrieved fungi on back of the photograph under the phylum, order, class, family, genera, and species using culture dependent method

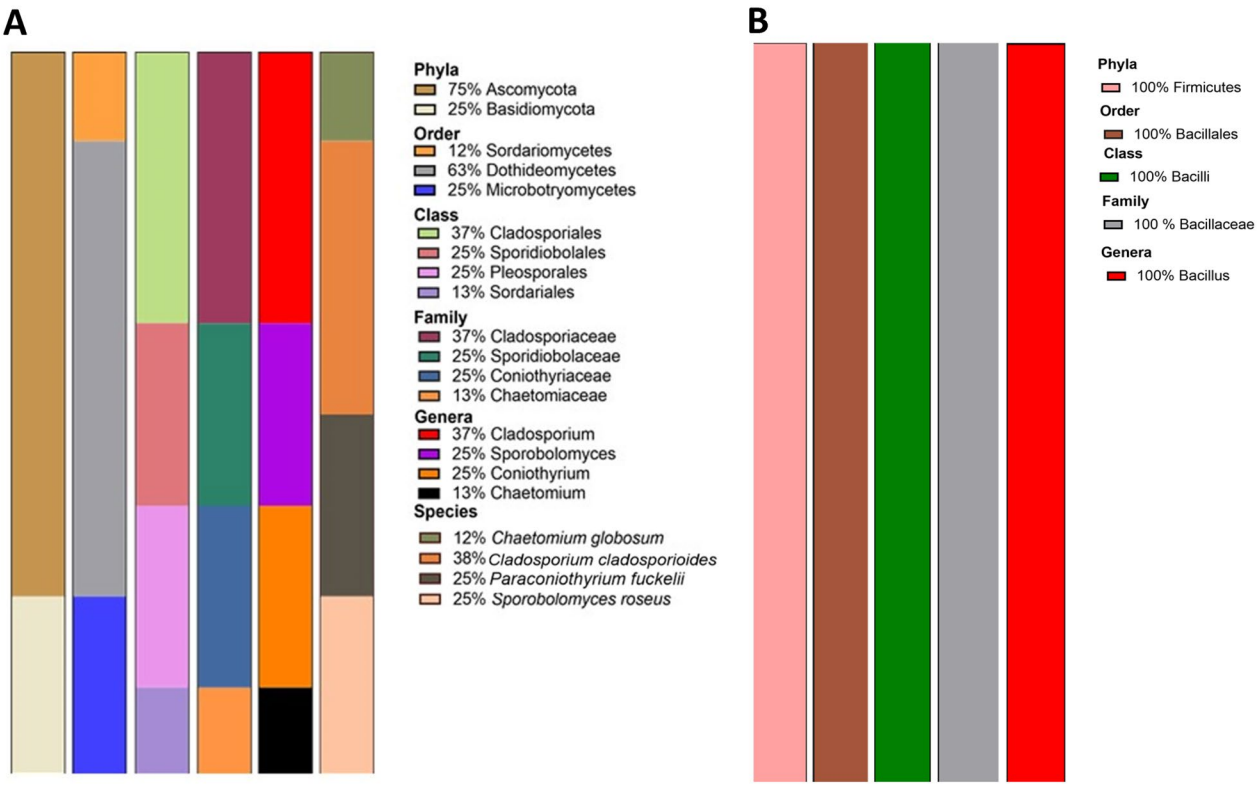

Fig. 3 Proportions of retrieved fungi on front of the photograph under the phylum, order, class, family, genera, and species using culture dependent method (**A**); proportions of retrieved bacteria on front canvas under the phylum, order, class, family, genera, and species using culture dependent method (**B**)

The ANalysis of SIMilarity (ANOSIM) test did not reveal statistical significance when samples were grouped based on the front and back localization of the canvas (16S, p-value 0.17; ITS2, p-value 0.28). However, significant values were observed when samples were analyzed individually, both for 16S and for ITS2 (p-values 0.001). Rarefaction plots to set sampling depth for alpha diversity are shown in Fig. 4.

Detailed relative abundances of Prokaryotes and fungi OTUs (from phylum to genus) are provided in Additional file 1: Tables S1 and S2. Subsequent bar plots for OTUs at the phylum and class levels are presented in Figs. 5–6 for Prokaryotes and fungi, respectively.

A total of 147 genera across 28 different classes of bacteria were identified, with 17 and 6 accounting for ≥ 1% of relative total abundance (RA_T), respectively (Additional file 1: Table S1). One hundred and two OTUs were excluded because they could not be verified at the genus level. Overall, 43 classes were well taxonomically identified, belonging to 18 phyla. Considering the $RA_T \geq 1\%$, this included 12 and 8, respectively (Fig. 5). The dominant phylum was Proteobacteria (37%), with Alphaproteobacteria and Gammaproteobacteria being the most representative classes (21.1% and 12.1%, respectively) in all sample from the photo (Fig. 5). Additionally, Betaproteobacteria was identified with a lower RA_T (3.5%). The Proteobacteria genera identified for all samples ($RA_T \geq 1\%$) were *Sphingomonas* (6.7%), *Enhydrobacter* (3.2%), *Paracoccus* (2.9%), *Erwinia* (2.7%), *Acinetobacter* (2.2%), *Pseudomonas* (1.8%), *Haemophilus* (0.8%), *Phyllobacterium* (0.8%) and *Methylobacterium* (0.6%). The phylum Cyanobacteria was also well represented by the class Oscillatoriophycideae with 18% (Fig. 5). The most represented family was Xenococcaceae (18%) with *Chroococcidiopsis* genus (13%). The genus *Calothrix* was present in only one sample (4 BC) with a lower relative abundance (RA) of 1%, while it was absent in two samples (6 FC, 2 BC) or in traces in the other samples. Overall, the observed bacterial diversity ($RA_T \geq 1$) did not show differences in composition but in the abundance of the sampled bacterial communities in Mapplethorpe's photograph. As previously mentioned, the composition of the fungal communities is shown in Fig. 6 and the relative abundances of fungal taxa are detailed in Additional file 1: Tables S2.

Fungal diversity at the phylum and genus levels was lower than that of the bacterial communities. Additionally, there were unassigned OTUs with a higher abundance compared to bacterial communities (Fig. 5 and

Table 1 Identification of microorganisms sampled from *Skull and Crossbones* photograph using ITS barcode. BC = back of the photograph; FC = front of the photograph

Species identification based on complete ITS barcode	Sampling point	Accession number
Paraconiothyrium fuckelii	BC	OR816146
Paraconiothyrium fuckelii	BC	OR816147
Chaetomium globosum	BC	OR816148
Cladosporium cladosporioides	FC	OR816149
Cladosporium cladosporioides	FC	OR816150
Cladosporium cladosporioides	FC	OR816151
Sporobolomyces roseus	FC	OR816152
Sporobolomyces roseus	FC	OR816153
Cladosporium ramotenellum	FC	OR816154
Cladosporium ramotenellum	FC	OR816155
Cladosporium ramotenellum	FC	OR816156
Cladosporium sphaerospermum	FC	OR816157
Cladosporium sphaerospermum	FC	OR816158
Penicillium chrysogenum	BC	OR816159
Penicillium chrysogenum	BC	OR816160
Penicillium chrysogenum	BC	OR816161
Penicillium chrysogenum	BC	OR816162
Purpureocillium lilacinum	BC	OR816163
Purpureocillium lilacinum	BC	OR816164
Bacillus sp.	FC	PP468626

Table 2 Deteriorative potential of fungal isolates derived from culture-dependent methods

Identified species	Cellulolytic activity	Proteolytic activity
Cladosporium cladosporioides	0.8 ± 0.1	+
Cladosporium ramotenellum	0.8 ± 0.1	–
Cladosporium sphaerospermum	0.9 ± 0.1	–
Sporobolomyces roseus	1.1 ± 0.1	–
Penicillium chrysogenum	1.7 ± 0.1	+
Purpureacilium liliacium	1.3 ± 0.1	+
Chaetomium globosum	1.0 ± 0.1	+
Paraconiothyrium fuckelii	0.9 ± 0.1	–

Fig. 6). This can be attributed to the marker's universality for certain eukaryotic taxa (i.e., Viridiplantae). A total of 135 genera across 14 different fungal classes were identified, with 16 and 8 accounting for ≥ 1% of the relative total abundance (RA_T), respectively. A significant portion of assigned fungi belonged to Ascomycota (49.9%), with Dothideomycetes as the dominant class with 33.1% of RA_T. The classes Eurotiomycetes, Sordariomycetes, and Leotiomycetes were identified with lower RA_T values (6.9, 4.9 and 2%, respectively). Saccharomycetes exhibited higher abundance in the front canvas (3.9% vs 1% back canvas). The dominant genera were *Cladosporium* (16.6%) and *Alternaria* (7%). Other genera with lower abundance but consistently observed in all sampling points included *Aspergillus* (2.4%) and *Penicillium* (1.8%). Considering an RA_T for ≥ 1%, genera variably present or in trace amounts in sampling points were: *Aureobasidium* (1.6%), *Stemphylium* (1.4%), *Gibberella* (1.2%), *Fusarium* and *Erysiphe* (0.9%), as well as *Hanseniaspora*, *Cadophora* (0.7%), and *Coniosporium* (0.6%) (Additional file 1: Table S2). *Hanseniaspora* was more abundant on the front canvas (FC) sampling points [2.3 vs 0.1% back canvas, (BC)].

The phylum Basidiomycota (26.1%) was well represented by the class Malasseziomycetes (RA_T = 18%), followed by Tremellomycetes and Agaricomycetes with lower RA_T values (6 and 2.2%, respectively) (Fig. 6). The most represented genus was *Malassezia* (16%), while *Dioszegia*, *Filobasidium* and *Vishniacozyma* (Tremellomycetes) were present at all points with lower relative abundance values (2.1 – 1.3%). Genera belonging to Agaricomycetes were well represented only in traces (*Peniophora*, *Trametes* and *Pleurotos*). Overall, the observed fungal diversity ($RA_T \geq 1$) did not show differences in composition but in the abundance of the sampled bacterial communities in Mapplethorpe photographs.

Additionally, among the other OTUs unidentified as fungi, Chlorophyta (Viridiplantae) was detected with the genus *Trebouxia* in all samples, with a variable abundance, more pronounced in the back of the photo (0.25 FC vs 0.8% BC) and *Coccomyxa* and *Acutodesmus* present only in trace amounts on the front canvas ($RA \leq 0.1\%$, data not shown).

Vibrational spectroscopies

Before delving into the results of the vibrational spectroscopic analysis of the gelatin-silver halide black and white prints, it is essential to note that the presence of various species, including both fungi and bacteria, on the photographic prints makes it challenging to conduct a detailed spectral analysis. This is because it becomes impossible to differentiate the contribution of each species. The examined prints were created on baryta papers, where silver halide salts were suspended in gelatin.

The Raman spectra of the microsamples taken from degraded and defaced areas on the front page of the photograph are presented in Fig. 7. The efflorescence in the spectra exhibit peaks at 1139, 990, 645, 620, 521, 458 cm^{-1}, which are associated with $BaSO_4$ [44], or baryte, the mineral situated between the support and the gelatin binder in gelatin prints. Additionally, signals in 1200–1720 cm^{-1} region may be attributed to gelatin and/or microorganisms: 1239 cm^{-1} (amide III) and

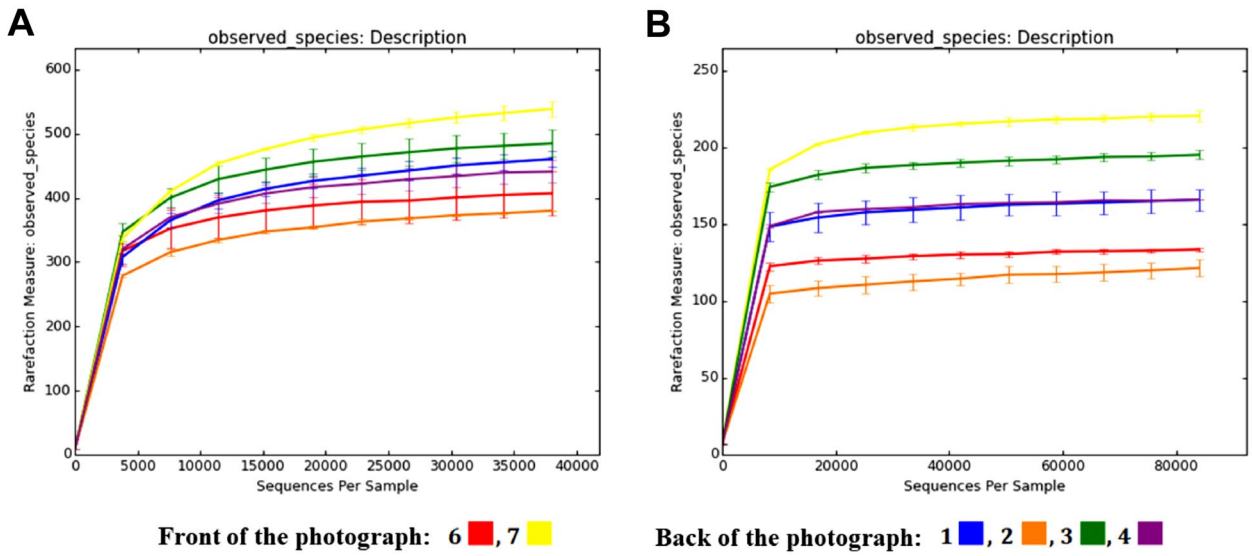

Fig. 4 Alpha rarefaction plots (observed species metric) per replicate for 16S (**A**) and ITS2 (**B**)

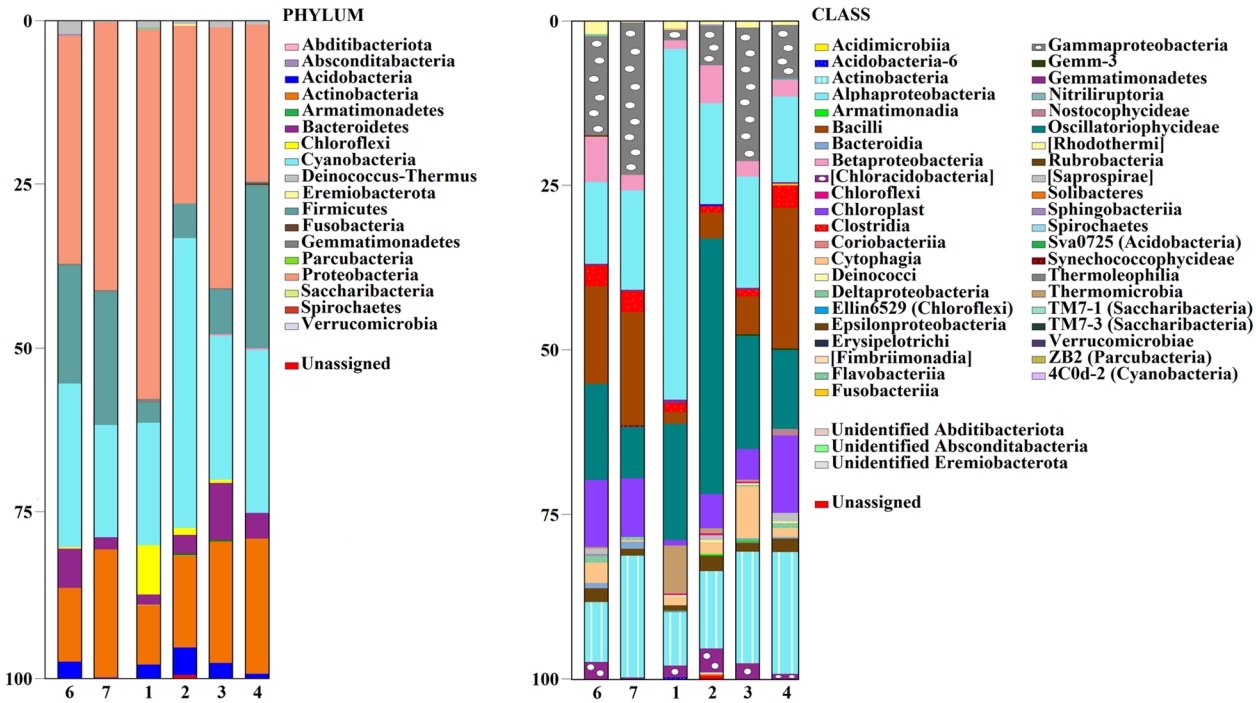

Fig. 5 Proportions prokaryotic operational taxonomic units (OTUs) under the phylum and class ranks using High-Throughput Sequencing data through metabarcoding analysis of 16S rRNA marker for the six tape samples [front of the photograph (FC):6, 7; back of the photograph (BC): 1, 2, 3, 4]. Further details for taxonomical level are provided in Additional file 1: Table S1

1650 cm^{-1} (amide I). Notably, neither barium phosphates (978 cm^{-1}) [45] nor anhydrite, $CaSO_4$ [46] were observed, in contrast to other cases of degradation.

The Raman spectrum of paper (Fig. 7) indicates the presence of non-acetylated cellulose (380, 1090, 1480 cm^{-1})[47].

Moreover, TiO_2 anatase features were detected (146, 384, 520, and 633 cm^{-1} corresponding to Eg, B1g, A1g,

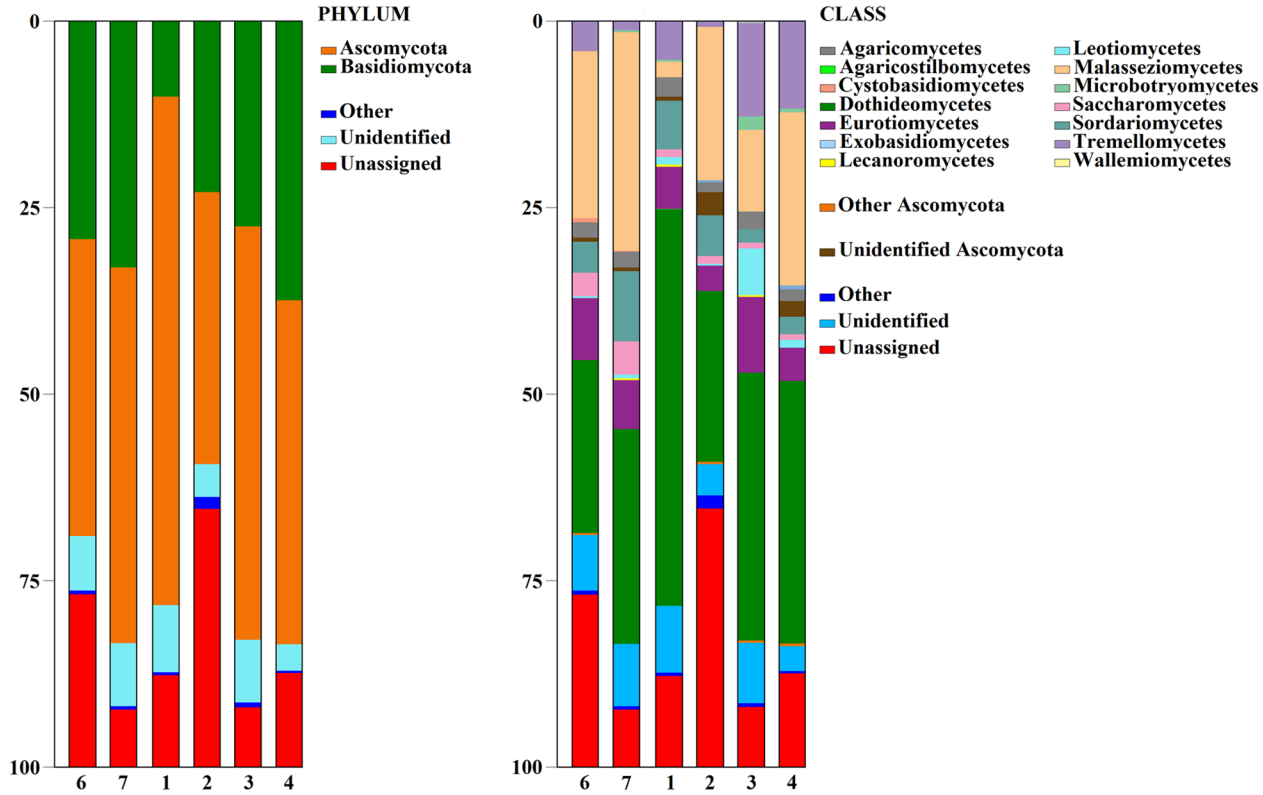

Fig. 6 Proportions fungal operational taxonomic units (OTUs) under the phylum and class ranks using High-Throughput Sequencing data through metabarcoding analysis of ITS2 nrDNA marker for the seven tape samples [front of the photograph (FC): 6, 7; back of the photograph (BC): 1, 2, 3, 4]. Further details for taxonomical level are provided in Additional file 1: Table S2

and Eg lattice vibration modes) without significant amount of titanates (which would be expected at 234, 660, and 1055 cm^{-1}), as elsewhere reported [40]. There was no detection of amorphous carbons (which typically appear around 1350 and 1660 cm^{-1}). Overall, Raman spectroscopy of the front of the photograph reveals only chemical component expected in the original photograph, without highlighting any direct chemical degradation, except for the extensive gelatin digestion induced by the microorganisms.

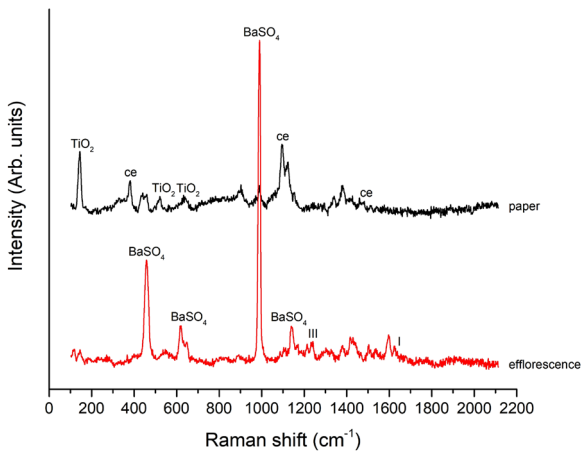

Fig. 7 Raman spectra of the microsampled degraded and defaced areas on the front of the photograph. Ce (cellulose), I (amide I) and III (amide III)

For the support on the back of the photograph, fluorescence hindered Raman acquisition, so FT-IR spectroscopy was employed. FT-IR spectra of white, yellow, and brown regions of the back of the photograph were collected in ATR mode and are presented in Fig. 8.

The white and yellow regions exhibited very similar FT-IR spectra, indicating the acetylation of the cellulose support [48, 49]. Conversely, the brown regions revealed only cellulose [50] and no longer exhibited the initial acetate coating. This evidence clearly indicates a stepwise degradation of the multilayer structure on the retro support of the photograph. The yellow areas reasonably underwent to a reversible microbial attachment on the acetate coating, whereas in the brown area microbiological degradation reached the support paper.

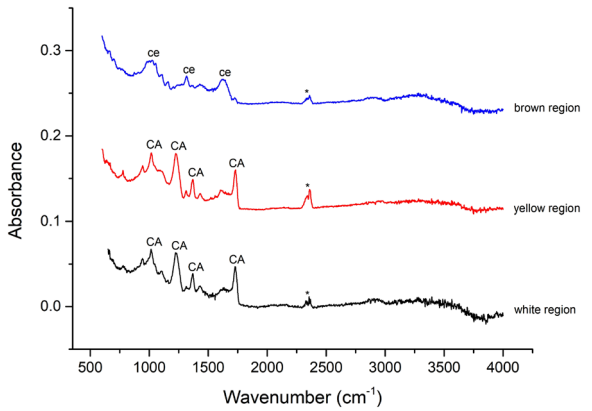

Fig. 8 ATR-FT-IR spectra of white, yellow, and brown regions of the back of the photograph. Ce (cellulose), CA (cellulose acetate). Star refers to carbon dioxide

Discussion

In this study, the microbial composition within "*Skull and Crossbones*," a significant photograph by Robert Mapplethorpe, was assessed. The identification of the associated microbiome found on both the front and back surfaces of the photograph was essential to evaluate its potential for causing degradation. Moreover, Raman and FT-IR measurements were respectively carried out on the front and the back of the photograph to assess the degree of chemical damage caused by the presence of the bacterial and fungal populations.

In detail, for the molecular analysis we selected the internal transcribed spacer (ITS 1–2) region, widely used as the official barcode for the molecular determination of fungal species and due to its ease of amplification and a well-defined barcode gap. Indeed, there is a vast amount of ITS data available on several International Nucleotide Sequence Databases (GenBank, EMBL and DDBJ). In particular, the entire ITS region or its subregions, namely ITS1 and ITS2, can be used as DNA barcoding markers for the Ascomycota and Basidiomycota phyla. However, the molecular identification success of the ITS region is higher in Basidiomycota than Ascomycota [51], primarily because some genera within the Ascomycota phylum, such as *Cladosporium* [52] and *Penicillium* [53], show narrow or no barcode gaps in the ITS sequence. Consequently, ITS may not offer sufficient variation to distinguish diverse fungal genera. Therefore, to achieve a deeper level of species identification, we used a combination of two other genes [54], β-tubulin and translation elongation factor 1-α (TEF1-α). The selection of these biomarkers was based on preliminary morphological data and the results obtained from ITS sequencing. ß-tubulin was chosen in accordance with established data recommending it as a secondary barcode for species identification in certain fungal genera, such as *Penicillium* and *Purpureocillium*, [55]. On the other hand, TEF1-α marker was used to confirm the identification of some of plant and human-pathogenic fungal strains retrieved in the present study, including Basidiomycota species and genera *Cladosporium*. Indeed, literature data show the higher specificity and discriminatory power of TEF1-α with respect to ITS [56]. The results obtained by combining ITS 1–2, ß-tubulin and TEF1-α markers are consistent with previous studies that have identified *Cladosporium cladosporiales*, *Cladosporium sphaerospermum*, *Penicillium chrysogenum*, *Purpureacillium liliacinum* and *Chaetomium globosum* as colonizers of photographic materials [57]. These fungi are well known for producing a wide range of enzymes, including proteinases and cellulases, which can degrade the components of photographic materials, including gelatin and paper [58]. For instance, the genus *Penicillium* can produce diffusive pigments and secrete malic and citric acid, along with cellulases, as reported for *P. chrysogenum* [59].

Chaetomium globosum produces various extracellular enzymes, including amylase, cellulase, laccase, lipase, pectinase, protease and chitinase [60]. Furthermore, most of these fungal species are commonly present in indoor environments, consequently constituting a serious risk to cellulose-based materials, such as photographs and canvas paintings. Indeed, under suitable conditions these microbes can initiate biodeterioration processes. Microbes in indoor environments can initiate biodeterioration processes under suitable conditions. Notably, genera like *Cladosporium* (Dothideomycetes), *Chaetomium* (Sordariomycetes), *Penicillium* (Eurotiomycetes) and *Purpureocilium* (Sordariomycetes) have been identified as xerophilic fungal organisms in indoor settings [61]. These fungi have the remarkable ability to produce a variety of pigments, including black, green, blue, purple, and violet, derived from different chemical classes like carotenoids, melanin, or quinones [62]. It is interesting to note that *Paracooniothyrium* (Ascomycota) and *Sporobolomyces* (Basidiomycota) which we identified within the microbiota of the *Skull and Crossbones* photograph have never previously reported as biodeteriogens-or simply inhabitants-of photographs or indoor works of art. However, both isolates displayed significant cellulolytic activity, suggesting their potential to deteriorate materials with high cellulose content. For instance, *Paraconiothyrium fuckelii* is a well-known soil and plant pathogen fungus [63, 64]. Similarly, *Sporobolomyces roseus* belongs to Uredimiomycetes, typical plant pathogens (rusts and smuts). Although these fungi may be opportunistic, we cannot confirm their origin and whether their presence is due to a particular level of specialization in using paint components or to a circumstantial deposit of spores

from the environment. To gain a better understanding of the microbial communities thriving on the *Skull and Crossbones* photograph, we also employed culture-independent methods to identify the species that could not be cultivated (i.e., Basidiomycetes). In particular, we used high-throughput sequencing (HTS) techniques that are ultra-sensitive and are excellent tools for accurate metagenomic studies. Such methods have already been successfully employed to investigate the microbial presence on photographic-based materials. Prokaryotes and fungal communities identified on Mapplethorpe's photo using HTS showed significant complexity. In comparison to similar studies conducted on objects stored at the Tianjin Museum [65], the bacterial biodiversity found was higher, although some trends, such as the dominant occurrence of Proteobacteria, Firmicutes, and Actinobacteria, were confirmed. The bacterial composition profile exhibited a closer resemblance to that found on objects from Crete Museum, as reported by Saridaki et al. [66]. At the genus level, the predominant presence of *Paracoccus*, one of the most abundant genera colonizing Mapplethorpe's photo, was observed, along with the occurrence of cyanobacteria belonging to Oscillatoriaceae. The unique characteristics of photographic materials may account for the distinctive composition of microbial communities, since surface characteristics influence their profile [12, 67]. *Enhydrobacter* is one of the major components of the community detected on silver gelatin photographs [68], and *Sphingomonas*, the most abundant genus found on Mapplethorpe's photograph, is a ubiquitous bacterium frequently isolated from various artifacts worldwide [69]. Even at low temperatures, it is capable of degrading proteinaceous substrates, such as gelatin or albumen, commonly used as photographic binders [70]. Overall, the most abundant bacteria identified on Mapplethorpe's artwork possess cellulolytic and proteolytic capabilities, potentially affecting the biodeterioration of photographic artworks.

The comparison between the results obtained from culture-dependent and culture-independent methods for bacteria detection is intriguing. The limited number of bacterial strains isolated from Mapplethorpe's photo may be attributed to a very low concentration of bacterial cells in the samples. The elevated levels of fungal contamination could potentially have contributed to a decline in bacterial concentration within the consortia. Additionally, it could be hypothesized that a significant portion of the bacterial components in the microbial population entered a resistance stage, limiting their growth potential in culture. An exception to this general pattern is the genus *Bacillus*, identified as the sole cultivable bacterium in the present study. Species within this genus typically produce spores capable of rapid growth in culture media [71]. Furthermore, this discrepancy may be elucidated by the limitations of culture-dependent methods, which can only identify 0.1–1% of microorganisms present on artworks. This small fraction of microorganisms thrives under laboratory cultivation conditions, enabling their isolation, while the rest may consist of undiscovered species or species in a viable but non-cultivable state (VBNC) for which suitable laboratory conditions cannot be established [72].

However, the discovery of *Bacillus* as a cultivable bacterium aligns with previous studies indicating that this genus is frequently isolated from audiovisual materials [2].

The fungal community structure retrieved on *The Skull and Crossbonnes* photograph predominantly featured the phylum Ascomycota, followed by Basidiomycota, as reported for many art objects affected by fungi, regardless of substrate characteristics, such as drawings [73], stones [74, 75], audio-visual materials [7]. At the genus level, the fungi identified in this work were also previously described as colonizing photographic materials [57]. The presence of a forested area around the building housing the *Terrae Motus* collection could account for the high prevalence of airborne fungi as *Cladosporium* and *Alternaria*. Furthermore, the significant occurrence of *Malassezia*, a human skin parasite, is likely associated with the high number of Museum visitors. *Cladosporium* spp. often form patinas or staining on gelatin positive print and negative films, as well as on the black and white albumen of paper photographs; a similar propension to colonize gelatin cellulose triacetate films was reported for *Alternaria*, particularly *A. alternata* [6] and *Malassezia*. *Malassezia* is one of the most frequently occurring genera in indoor samples of museum exhibition rooms [76]. Consistent with Sanger sequencing results, HTS results also showed a higher presence of Ascomycota species than Basidiomycota. Other genera within the Ascomycota were also detected, such as *Alternaria*, *Aspergillus,* and *Fusarium,* which are commonly found in association with various works of art of historical and cultural heritage. Despite the high frequency of the Ascomycota phylum, HTS sequencing revealed a significant presence of the Basidiomycota phylum. Among Basidiomycota, the most abundant genus was *Malassezia*, which was not detected using culture-dependent methods. *Malassezia*, is a well-known dermatophyte opportunistic fungus, commonly associated with human skin as a causative agent of skin-related issues such as dandruff and seborrheic dermatitis. It is also found within other warm-blooded animals [77]. Although *Malassezia* is an unusual contaminant in cultural heritage, recent studies have revealed its unexpected presence on cultural

heritage artifacts, such as ancient manuscripts, paintings, sculptures, photograph, and textiles [78, 79]. The presence of this fungus on such objects poses new challenges for conservators and researchers due to its ability to degrade cellulose and produce lipolytic enzymes [80]. Furthermore, its spores could easily spread into the surrounding closed environment where photograph is exposed, representing a serious health concern for visitors, restorers, and museum workers. The discovery of *Malassezia* on cultural heritage artifacts emphasizes the importance of continuous research and vigilance in the field of heritage preservation.

Lastly, the presence of taxa belonging to Anthophyta in trace amounts was also observed (data not shown), likely due to airborne or human contamination.

Overall, the presence of these described fungi in photographic materials and their ability to degrade cellulose and protein in vitro demonstrate that these microorganisms could be responsible for the degradation and appearance of foxing in historical photograph. All isolates in this study showed cellulolytic activity, while not all microorganisms showed proteolytic activity.

Finally, to evaluate the chemical degradation conditions, we used vibrational spectroscopies [81, 82]. In particular, the FT-IR analysis on the back of the photograph allowed to correlate the different colors of the cellulose support with different degradation stage, in terms of loss of its acetate coating. Conversely, the Raman analysis shows that the extensive microbial digestion of the gelatin at the front of the photograph is not accompanied by any direct chemical degradation.

Understanding the factors contributing to fungal infestation on cultural heritage artifacts and the consequent degradation is crucial for implementing effective mitigation strategies, considering the presence of organic residues, and environmental conditions promoting fungal proliferation. Additionally, environmental conditions, such as temperature and humidity fluctuations, may play a role in promoting fungal proliferation on vulnerable artifacts. The handling, exposure and storage conditions of artwork inhabited by human opportunistic pathogenic fungi should be evaluated with care, continuously monitored and, if necessary, improved. By understanding the implications of fungal infestations and implementing effective mitigation strategies, conservators can better safeguard these precious objects for future generations.

Conclusions

Even though museums of significant historical relevance, such as the Royal Palace of Caserta, maintain controlled indoor environment, fluctuations in relative humidity and temperature can still occur, potentially leading to the attachment of microorganisms, particularly fungi, on exhibited works of art. In addition, it is important to consider that the large number of visitors can facilitate the introduction of microorganism into the museum, which can contribute to chemical, physical, mechanical, or aesthetic degradation of the artworks. The combined application of molecular and spectroscopic methods has proven to be a valuable tool for understanding not only the composition and function of microbial communities colonizing ancient photographic material but also the extent of chemical alteration of the photograph under investigation. These findings can assist in identifying resilient microbes on the substrate, enabling the establishment of strategic interventions to control the museum's climatic conditions and visitor flow. Additionally, it is essential to continuously monitor the structure, composition, and activity of microbial communities to assess the impacts of control measures or conservation treatments. Therefore, the development of a standardized approach to investigate biodeterioration issues is desirable.

Abbreviations

HTS	High Throughput Sequencing
FT-IR	Fourier-transform infrared spectroscopy
BC	Back canvas
FC	Front canvas
FCUF	Fungal collection university of Naples Federico II
PDA	Potato dextrose agar
TSA	Tryptone soy agar
CMC	Carboxymethyl cellulose
EI	Enzymatic index
OTUs	Operational Taxonomic Units
ITS	Internal transcribed spacer
BTUB	B-tubulin
TEF1	Translation elongation factor 1
ANOSIM	Analysis of similarity

Supplementary Information

The online version contains supplementary material available at https://doi.org/10.1186/s40494-024-01261-x.

Additional file 1: Appendix S1. DNA Extraction from adhesive tape. **Table S1.** List of prokaryotic Operational Taxonomic Units (OTUs) identified using high-throughput sequencing data through metabarcoding analysis of 16S rRNA marker, showing relative frequencies per sample [front canvas (FC): 5, 6; back canvas (BC): 1, 2, 3, 4]. **Table S2.** List of fungal Operational Taxonomic Units (OTUs) identified using high-throughput sequencing data through metabarcoding analysis of ITS2 nrDNA marker, showing relative frequencies per sample [front canvas (FC): 6, 7; back canvas (BC): 1, 2, 3, 4].

Acknowledgements

Not applicable

Author contributions

MP: concept proposal, main writer, main experimental performers, analysis, and interpretation of results, preparation of Figs. 2, 3 and tables; ADN: sampling data collection, preparation of Fig. 1; ADM sampling data collection, reviewer; RT: chemical measurements, preparation of Figs. 7 and 8; ODC: analysis and interpretation of HTS, reviewer; NM: HTS experiments; MA: preparation of Figs. 4, 5 and 6, statistical analysis; GT: head of the palatine library, historical

archives, photography, digitalization; GOG: care of the historical and artistic heritage; AV: funding acquisition, experimental design, reviewer; AP funding acquisition, experimental design, analysis of results, reviewer. All authors discussed the research outcome, as well as approved the final manuscript.

Funding
This work was financially supported by PNRR PE5 Changes (PE00000020).

Availability of data and materials
The datasets supporting the conclusions of this article are included within the article (and its additional files). Raw reads are available at NCBI Bioproject ID PRJNA1037003.

Declarations

Competing interests
The authors declare no competing interests.

Received: 7 December 2023 Accepted: 26 April 2024
Published online: 29 May 2024

References

1. Osman ME, Ismael S, Ciliberto E, Stefani S, Elsaba YM. Evaluation of microbial deterioration of silver gelatin photographs stored in an old photographic archive. Int J Cons Sci. 2022;13(2):527–40.
2. Tepla B, Demnerova K, Stiborova H. History and microbial biodeterioration of audiovisual materials. J Cult Herit. 2020;44:218–28. https://doi.org/10.1016/j.culher.2019.12.009.
3. Abrusci C, Marquina D, Del Amo A, Catalina F. Biodegradation of cinematographic gelatin emulsion by bacteria and filamentous fungi using indirect impedance technique. Int Biodeterior Biodegrad. 2007;60(3):137–43. https://doi.org/10.1016/j.ibiod.2006.06.011.
4. Abrusci C, Martín-González A, Del Amo A, Catalina F, Collado J, Platas G. Isolation and identification of bacteria and fungi from cinematographic films. Int Biodeterior Biodegrad. 2005;56(1):58–68. https://doi.org/10.1016/j.ibiod.2005.05.004.
5. Puškárová A, Bučková M, Habalová B, Kraková L, Maková A, Pangallo D. Microbial communities affecting albumen photography heritage: a methodological survey. Sci Rep. 2016;6(1):20810. https://doi.org/10.1038/srep20810.
6. Kosel J, Ropret P. Overview of fungal isolates on heritage collections of photographic materials and their biological potency. J Cult Herit. 2021;48:277–91. https://doi.org/10.1016/j.culher.2021.01.004.
7. Branysova T, Demnerova K, Durovic M, Stiborova H. Microbial biodeterioration of cultural heritage and identification of the active agents over the last two decades. J Cult Herit. 2022;55:245–60. https://doi.org/10.1016/j.culher.2022.03.013.
8. Zamboni CB, Redígolo MM, Miura VT, Costa I, Nagai MLE, Salvador PAV, et al. Non-destructive analysis in the study of historical photographs by pXRF and ATR-FTIR spectroscopies. J Forens Sci. 2021;66(3):1048–55. https://doi.org/10.1111/1556-4029.14680.
9. Szulc J, Okrasa M, Dybka-Stępień K, Sulyok M, Nowak A, Otlewska A, et al. Assessment of microbiological indoor air quality in cattle breeding farms. Aerosol Air Qual Res. 2020;20(6):1353–73. https://doi.org/10.4209/aaqr.2019.12.0641.
10. Kosel J, Kavčič M, Legan L, et al. Evaluating the xerophilic potential of moulds on selected egg tempera paints on glass and wooden supports using fluorescent microscopy. J Cult Herit. 2021;52:44–54.
11. Purkrtova S, Savicka D, Kadava J, Sykorova H, Kovacova N, Kalisova D, et al. Microbial contamination of photographic and cinematographic materials in archival funds in the czech republic. Microorganisms. 2022;10(1):155. https://doi.org/10.3390/microorganisms10010155.
12. Bučková M, Puškárová A, Sclocchi MC, Bicchieri M, Colaizzi P, Pinzari F, et al. Co-occurrence of bacteria and fungi and spatial partitioning during photographic materials biodeterioration. Polym Degrad Stab. 2014;108:1–11. https://doi.org/10.1016/j.polymdegradstab.2014.05.025.
13. Marvasi M, Cavalieri D, Mastromei G, Casaccia A, Perito B. Omics technologies for an in-depth investigation of biodeterioration of cultural heritage. Int Biodeterior Biodegrad. 2019;144: 104736. https://doi.org/10.1016/j.ibiod.2019.104736.
14. Rosado T, Mirão J, Candeias A, Caldeira AT. Microbial communities analysis assessed by pyrosequencing—a new approach applied to conservation state studies of mural paintings. Anal Bioanal Chem. 2014;406(3):887–95. https://doi.org/10.1007/s00216-013-7516-7.
15. Trovão J, Portugal A. Current knowledge on the fungal degradation abilities profiled through biodeteriorative plate essays. Appl Sci. 2021;11(9):4196. https://doi.org/10.1016/j.ibiod.2019.05.008.
16. Marucci G, Monno A, Van Der Werf ID. Non invasive micro-Raman spectroscopy for investigation of historical silver salt gelatin photographs. Microchem J. 2014;117:220–4. https://doi.org/10.1016/j.microc.2014.07.001.
17. Pelosi C, Di Stasio F, Lanteri L, Zuena M, Sardara M, Sodo A. The, "restoration of the restoration": investigation of a complex surface and interface pattern in the roman wall paintings of Volsinii Novi (Bolsena, central Italy). Coatings. 2024;14(4):408. https://doi.org/10.3390/coatings14040408.
18. Kujović A, Gostinčar C, Kavkler K, Govedić N, Gunde-Cimerman N, Zalar P. Degradation potential of xerophilic and xerotolerant fungi contaminating historic canvas paintings. JoF. 2024;10(1):76. https://doi.org/10.3390/jof10010076.
19. Berger Haladová Z, Bohdal R, Černeková Z, Štancelová P, Ferko A, Blaško Križanová J, et al. Finding the best lighting mode for daguerreotype, ambrotype, and tintype photographs and their deterioration on the cruse scanner based on selected methods. Sensors. 2023;23(4):2303. https://doi.org/10.3390/s23042303.
20. Osman ME, Ismael S, Ciliberto E, Stefani S, Elsaba YM. Evaluation of microbial deterioration of silver gelatin photographs stored in an old photographic archive. Int J Conserv Sci. 2022;13(2):527–40.
21. Shaheen R, Fouad M, Saqr O, Reda S, Labeeb A. Assessment of the photo-chemical degradation of silver gelatin photograph print-out. Int J Conserv Sci. 2020;11(4):1093–102.
22. Lourenço MJL, Sampaio JP. Microbial deterioration of gelatin emulsion photographs: Differences of susceptibility between black and white and color materials. Int Biodeterior Biodegrad. 2009;63(4):496–502. https://doi.org/10.1016/j.ibiod.2008.10.011.
23. Petraretti M, Duffy KJ, Del Mondo A, Pollio A, De Natale A. Community composition and ex situ cultivation of fungi associated with UNESCO heritage monuments in the Bay of Naples. Appl Sci. 2021;11(10):4327. https://doi.org/10.3390/app11104327.
24. Doyle JJ, Doyle JL. Isolation of plant DNA from fresh tissue. Focus. 1990;12:13–5.
25. Del Mondo A, De Natale A, Pinto G, Pollio A. Correction to: novel qPCR probe systems for the characterization of subaerial biofilms on stone monuments. Ann Microbiol. 2019;69(10):1097–106. https://doi.org/10.1007/s13213-019-01480-9.
26. White TJ, Bruns T, Lee SJW, Taylor J. Amplification, and direct sequencing of fungal ribosomal RNA genes for phylogenetics. PCR protoc guid method appl. 1990;18(1):315–22.
27. Visagie CM, Houbraken J, Frisvad JC, Hong SB, Klaassen CHW, Perrone G, et al. Identification and nomenclature of the genus *Penicillium*. Stud Mycol. 2014;78(1):343–71. https://doi.org/10.1016/j.simyco.2014.09.001.
28. Carbone I, Anderson JB, Kohn LM. Patterns of descent in clonal lineages and their multilocus fingerprints are resolved with combined gene genealogies. Evolution. 1999;53(1):11–21. https://doi.org/10.1111/j.1558-5646.1999.tb05329.x.
29. Cutler NA, Oliver AE, Viles HA, Whiteley AS. Non-destructive sampling of rock-dwelling microbial communities using sterile adhesive tape. J Microbiol Method. 2012;91(3):391–8. https://doi.org/10.1016/j.mimet.2012.09.022.
30. Takahashi S, Tomita J, Nishioka K, Hisada T, Nishijima M. Development of a prokaryotic universal primer for simultaneous analysis of bacteria and archaea using next-generation sequencing. PLoS ONE. 2014;9(8):e105592. https://doi.org/10.1371/journal.pone.0105592.
31. Carroll NM, Adamson P, Okhravi N. Elimination of bacterial DNA from *Taq* DNA polymerases by restriction endonuclease digestion. J Clin Microbiol. 1999;37(10):3402–4. https://doi.org/10.1128/JCM.37.10.3402-3404.1999.

32. Zhang J, Kobert K, Flouri T, Stamatakis A. PEAR: a fast and accurate illumina paired-end reAd mergeR. Bioinformatics. 2014;30(5):614–20. https://doi.org/10.1007/s11274-011-0919-8.
33. Bengtsson-Palme J, Ryberg M, Hartmann M, Branco S, Wang Z, Godhe A, et al. Improved software detection and extraction of ITS1 and ITS 2 from ribosomal ITS sequences of fungi and other eukaryotes for analysis of environmental sequencing data. Method Ecol Evol. 2013;4(10):914–9. https://doi.org/10.1111/2041-210X.12073.
34. Rognes T, Flouri T, Nichols B, Quince C, Mahé F. VSEARCH: a versatile open source tool for metagenomics. PeerJ. 2016;4: e2584. https://doi.org/10.7717/peerj.2584.
35. Edgar RC, Haas BJ, Clemente JC, Quince C, Knight R. UCHIME improves sensitivity and speed of chimera detection. Bioinformatics. 2011;27(16):2194–200. https://doi.org/10.1093/bioinformatics/btr381.
36. Caporaso JG, Kuczynski J, Stombaugh J, Bittinger K, Bushman FD, Costello EK, et al. QIIME allows analysis of high-throughput community sequencing data. Nat Method. 2010;7(5):335–6. https://doi.org/10.1038/nmeth.f.303.
37. Fierer N, Lauber CL, Zhou N, McDonald D, Costello EK, Knight R. Forensic identification using skin bacterial communities. Proc Natl Acad Sci USA. 2010;107(14):6477–81. https://doi.org/10.1073/pnas.1000162107.
38. Gupta P, Samant K, Sahu A. Isolation of cellulose-degrading bacteria and determination of their cellulolytic potential. Int J Microbiol. 2012;2012:1–5. https://doi.org/10.1016/j.jaad.2003.12.034.
39. Florencio C, Couri S, Farinas CS. Correlation between agar plate screening and solid-state fermentation for the prediction of cellulase production by trichoderma strains. Enzyme Res. 2012;2012:1–7. https://doi.org/10.1155/2012/793708.
40. Bourne R. ImageJ. In: Fundamentals of digital imaging in medicine. London: Springer, London; 2010. p. 185–8.
41. Borrego S, Guiamet P, Gómez De Saravia S, Batistini P, Garcia M, Lavin P, et al. The quality of air at archives and the biodeterioration of photographs. Int Biodeterior Biodegrad. 2010;64(2):139–45. https://doi.org/10.1016/j.ibiod.2009.12.005.
42. Vermelho AB, Meirelles MNL, Lopes A, Petinate SDG, Chaia AA, Branquinha MH. Detection of extracellular proteases from microorganisms on agar plates. Mem Inst Oswaldo Cruz. 1996;91(6):755–60. https://doi.org/10.1590/S0074-02761996000600020.
43. Vergara A, Vitagliano L, Merlino A, Sica F, Marino K, Verde C, et al. An order-disorder transition plays a role in switching off the root effect in fish hemoglobins. J Biol Chem. 2010;285(42):32568–75. https://doi.org/10.1074/jbc.M110.143537.
44. Buzgar, N., Apopei, A.I., Buzatu,A. Romanian database of raman spectroscopy. 2009. http://rdrs.uaic.ro
45. Sclocchi MC, Kraková L, Pinzari F, Colaizzi P, Bicchieri M, Šaková N, et al. Microbial life and death in a foxing stain: a suggested mechanism of photographic prints defacement. Microb Ecol. 2017;73(4):815–26. https://doi.org/10.1007/s00248-016-0913-7.
46. Bergamonti L, Cirlini M, Graiff C, Lottici PP, Palla G, Casoli A. Characterization of waxes in the roman wall paintings of the herculaneum site (Italy). Appl Sci. 2022;12(21):11264. https://doi.org/10.3390/app122111264.
47. Agarwal UP, Ralph SA, Baez C, Reiner RS. Detection and quantitation of cellulose ii by raman spectroscopy. Cellulose. 2021;28(14):9069–79. https://doi.org/10.1007/s10570-021-04124-x.
48. Lavédrine B, Lavédrine J, Gandolfo JP, Lavédrine P, Monod S. A guide to the preventive conservation of photograph collections. Los Angeles: Getty Publications; 2003.
49. Amara M, Arous O, Smail F, Kerdjoudj H, Trari M, Bouguelia A. An assembled poly-4-vinyl pyridine and cellulose triacetate membrane and Bi2S3 electrode for photoelectrochemical diffusion of metallic ions. J Hazard Mater. 2009;169(1–3):195–202. https://doi.org/10.1016/j.jhazmat.2009.03.085.
50. Garside P, Wyeth P. Identification of cellulosic fibres by FTIR spectroscopy-thread and single fibre analysis by attenuated total reflectance. Stud Conserv. 2003;48(4):269–75. https://doi.org/10.1179/sic.2003.48.4.269.
51. Seifert KA. Progress towards DNA barcoding of fungi. Mol Ecol Resour. 2009;9(s1):83–9. https://doi.org/10.1111/j.1755-0998.2009.02635.x.
52. Schoch CL, Seifert KA, Huhndorf S, Robert V, Spouge JL, Levesque CA, et al. Nuclear ribosomal internal transcribed spacer (ITS) region as a universal DNA barcode marker for *Fungi*. Proc Natl Acad Sci USA. 2012;109(16):6241–6. https://doi.org/10.1073/pnas.1117018109.
53. Stielow JB, Lévesque CA, Seifert KA, Meyer W, Irinyi L, Smits D, et al. One fungus, which genes? development and assessment of universal primers for potential secondary fungal DNA barcodes. Pers Int Mycol J. 2015;35(1):242–63. https://doi.org/10.3767/003158515X689135.
54. Begerow D, John B, Oberwinkler F. Evolutionary relationships among β-tubulin gene sequences of basidiomycetous fungi. Mycol Res. 2004;108(11):1257–63. https://doi.org/10.1017/S0953756204001066.
55. Visagie CM, Seifert KA, Houbraken J, Samson RA, Jacobs K. A phylogenetic revision of penicillium sect. exilicaulis, including nine new species from fynbos in South Africa. IMA Fung. 2016;7(1):75–117. https://doi.org/10.5598/imafungus.2016.07.01.06.
56. Mirhendi H, Makimura K, De Hoog GS, Rezaei-Matehkolaei A, Najafzadeh MJ, Umeda Y, et al. Translation elongation factor 1-α gene as a potential taxonomic and identification marker in dermatophytes. Med Mycol. 2015;53(3):215–24. https://doi.org/10.1093/mmy/myu088.
57. Szulc J, Ruman T, Karbowska-Berent J, Kozielec T, Gutarowska B. Analyses of microorganisms and metabolites diversity on historic photographs using innovative methods. J Cult Herit. 2020;45:101–13. https://doi.org/10.1016/j.culher.2020.04.017.
58. Abrusci C, Marquina D, Del Amo A, Corrales T, Catalina F. A viscometric study of the biodegradation of photographic gelatin by fungi isolated from cinematographic films. Int Biodeterior Biodegrad. 2006;58(3–4):142–9. https://doi.org/10.1016/j.ibiod.2007.01.005.
59. Suphaphimol N, Suwannarach N, Purahong W, Jaikang C, Pengpat K, Semakul N, et al. Identification of microorganisms dwelling on the 19th century lanna mural paintings from northern thailand using culture-dependent and -independent approaches. Biology. 2022;11(2):228. https://doi.org/10.3390/biology11020228.
60. Abdel-Azeem AM, Gherbawy YA, Sabry AM. Enzyme profiles and genotyping of *Chaetomium globosum* isolates from various substrates. Plant Biosyst Int J Deal Aspect Plant Biol. 2016;150(3):420–8. https://doi.org/10.1080/11263504.2014.984791.
61. Trovão J, Portugal A, Soares F, Paiva DS, Mesquita N, Coelho C, et al. Fungal diversity and distribution across distinct biodeterioration phenomena in limestone walls of the old cathedral of Coimbra, UNESCO World Heritage Site. Int Biodeterior Biodegrad. 2019;142:91–102. https://doi.org/10.3390/app11094196.
62. Melo D, Sequeira SO, Lopes JA, Macedo MF. Stains versus colourants produced by fungi colonising paper cultural heritage: a review. J Cult Herit. 2019;35:161–82. https://doi.org/10.1016/j.culher.2018.05.013.
63. Wang J, Shao S, Liu C, Song Z, Liu S, Wu S. The genus *Paraconiothyrium*: species concepts, biological functions, and secondary metabolites. Crit Rev Microbiol. 2021;47(6):781–810. https://doi.org/10.1080/1040841X.2021.1933898.
64. Tennakoon DS, Thambugala KM, Silva NID, Suwannarach N, Lumyong S. A taxonomic assessment of novel and remarkable fungal species in didymosphaeriaceae (pleosporales, dothideomycetes) from plant litter. Front Microbiol. 2022;13:1016285. https://doi.org/10.3389/fmicb.2022.1016285.
65. Liu Z, Zhang Y, Zhang F, Hu C, Liu G, Pan J. Microbial community analyses of the deteriorated storeroom objects in the tianjin museum using culture-independent and culture-dependent approaches. Front Microbiol. 2018;9:802. https://doi.org/10.3389/fmicb.2018.00802.
66. Saridaki A, Katsivela E, Glytsos T, Tsiamis G, Violaki E, Kaloutsakis A, et al. Identification of bacterial communities on different surface materials of museum artefacts using high throughput sequencing. J Cult Herit. 2022;54:44–52. https://doi.org/10.1016/j.culher.2022.01.010.
67. Torralba MG, Kuelbs C, Moncera KJ, Roby R, Nelson KE. Characterizing microbial signatures on sculptures and paintings of similar provenance. Microb Ecol. 2021;81(4):1098–105. https://doi.org/10.1007/s00248-020-01504-x.
68. Pyzik A, Ciuchcinski K, Dziurzynski M, Dziewit L. The bad and the good—microorganisms in cultural heritage environments—an update on biodeterioration and biotreatment approaches. Materials. 2021;14(1):177. https://doi.org/10.3390/ma14010177.
69. Zhu C, Wang B, Tang M, Wang X, Li Q, Hu Y, et al. Analysis of the microbiomes on two cultural heritage sites. Geomicrobiol J. 2023;40(2):203–12. https://doi.org/10.1080/01490451.2022.2137604.
70. Kisová Z, Planý M, Pavlović J, Bučková M, Puškárová A, Kraková L, et al. Biodeteriogens characterization and molecular analyses of diverse funeral

accessories from XVII century. Appl Sci. 2020;10(16):5451. https://doi.org/10.3390/app10165451.
71. Laiz L, Piñar G, Lubitz W, Saiz-Jimenez C. The colonisation of building materials by microorganisms as revealed by culturing and molecular methods. In: Laiz L, Piñar G, Lubitz W, Saiz-Jimenez C, editors. Molecular biology and cultural heritage. Routledge: New York; 2003. p. 23–8.
72. Gutarowska B. The use of -omics tools for assessing biodeterioration of cultural heritage a review. J Cult Herit. 2020. https://doi.org/10.1016/j.culher.2020.03.006.
73. Piñar G, Sclocchi MC, Pinzari F, Colaizzi P, Graf A, Sebastiani ML, et al. The microbiome of leonardo da vinci's drawings: a bio-archive of their history. Front Microbiol. 2020;11: 593401. https://doi.org/10.3389/fmicb.2020.593401.
74. Li Q, Zhang B, He Z, Yang X. Distribution and diversity of bacteria and fungi colonization in stone monuments analyzed by high-throughput sequencing. PLoS ONE. 2016;11(9): e0163287. https://doi.org/10.1371/journal.pone.0163287.
75. Negi A, Sarethy IP. Microbial biodeterioration of cultural heritage: events, colonization, and analyses. Microb Ecol. 2019;78(4):1014–29. https://doi.org/10.1007/s00248-019-01366-y.
76. Saridaki A, Glytsos T, Raisi L, Katsivela E, Tsiamis G, Kalogerakis N, et al. Airborne particles, bacterial and fungal communities insights of two museum exhibition halls with diverse air quality characteristics. Aerobiologia. 2023;39(1):69–86. https://doi.org/10.1007/s10453-022-09775-2.
77. Gupta AK, Batra R, Bluhm R, Boekhout T, Dawson TL. Skin diseases associated with Malassezia species. J Am Acad Dermatol. 2004;51(5):785–98. https://doi.org/10.1155/2012/578925.
78. Cappa F, Piñar G, Brenner S, Frühmann B, Wetter W, Schreiner M, et al. The kiev folia: an interdisciplinary approach to unravelling the past of an ancient slavonic manuscript. Int Biodeterior Biodegrad. 2022;167: 105342. https://doi.org/10.1016/j.ibiod.2021.105342.
79. Pinheiro C, Miller AZ, Vaz P, Caldeira AT, Casanova C. Underneath the purple stain. Heritage. 2022;5(4):4100–13. https://doi.org/10.3390/heritage5040212.
80. Hossain H, Landgraf V, Weiss R, Mann M, Hayatpour J, Chakraborty T, et al. Genetic and biochemical characterization of *Malassezia pachydermatis* with particular attention to pigment-producing subgroups. Med Mycol. 2007;45(1):41–9. https://doi.org/10.1080/13693780601003827.
81. Cattaneo B, Chelazzi D, Giorgi R, Serena T, Merlo C, Baglioni P. Physico-chemical characterization and conservation issues of photographs dated between 1890 and 1910. J Cult Herit. 2008;9:277–84. https://doi.org/10.1016/j.culher.2008.01.004.
82. Casoli A, Fornaciari S. An analytical study on an early twentieth-century Italian photographs collection by means of microscopic and spectroscopic techniques. Microchem J. 2014;116:24–30. https://doi.org/10.1016/j.microc.2014.04.003.

Publisher's Note